ELSEVIER

Contents lists available at ScienceDirect

International Journal of Non-Linear Mechanics

journal homepage: www.elsevier.com/locate/nlm



Two-dimensional granular-thin plate interface for shock mitigation

Chongan Wang a,*, Sameh Tawfick a,b, Alexander F. Vakakis a

- ^a Department of Mechanical Science and Engineering, University of Illinois, Urbana, United States of America
- b The Beckman Institute for Advanced Science and Technology, University of Illinois, Urbana, United States of America



ARTICLE INFO

Dedicated to the memory of Prof. Leonid I. Manevitch

Keywords: Shock mitigation Granular-solid interface Nonlinear wave propagation

ABSTRACT

The efficacy for shock mitigation of an interface between a hexagonally-packed ordered granular medium and an elastic solid — referred to as the "granular-solid interface", is studied. The granular medium is composed of three columns of granules (with the intermediate column composed of "intruders", i.e., of lighter granules compared to their neighbors) which are closely packed but without any initial precompression. The granular medium is in contact with a thin plate (the elastic solid) in plane stress so that only planar motions are considered. This yields a strongly nonlinear, hybrid, i.e., discrete-continuum 2D acoustical problem. A half -sine distributed shock is applied to the left granular column, and the aim is to mitigate as much as possible the shock energy transmitted to the thin plate. The discrete element (DE) method is adopted to model the granular responses which incorporate not only Hertzian (normal) contact interactions, but also frictional effects due to granule rotations. A computational algorithm based on interpolations and iterations is employed to accurately simulate the contact forces at the interface between the granular medium and the thin plate, modeled using finite element, and the numerical stability is checked at each successive (variable) time step to ensure unconditional convergence of the numerical results. It is shown that the granular medium can be designed to absorb a major portion of the applied impulsive energy. To this end a study of the energy partition in the granular interface is performed by changing the sizes and material properties of the column of intruders, and investigating the amount of impulsive energy that is eventually transmitted to the thin plate. When lighter polytetrafluoroethylene (PTFE) intruders are combined with heavier steel granules, it is shown that the impulsive energy is mostly localized in the first column of the granular medium and negligible energy reaches the thin plate. The reason for this effective shock mitigation is the disparity in the time scales between the responses of the steel granules and the PTFE intruders, which, in turn, leads to an effective impedance mismatch that confines the impulsive energy, preventing it from propagating through the interface. Moreover, being nonlinear, the shock mitigation effectiveness of the granular-solid interface is tunable with energy, with enhanced effectiveness for weaker shocks. The methods and results reported in this work pave the way for predictively designing hybrid interfaces for drastically enhanced shock mitigation, with broad engineering applications.

1. Introduction

Wave propagation in granular media composed of closely packed ordered granules has attracted considerable attention of researchers. The geometric nonlinearity of the contact constitutive law enables rich nonlinear phenomenon in granular media. Nesterenko et al. [1–5] pioneered the research of wave propagation in ordered granular media composed of identical linear elastic granules ordered and having no initial pre-compression. Solitary waves (referred to as Nesterenko solitary waves) are realized in homogeneous one-dimensional (1D) granular chains, having the form of localized pulses that preserve their shapes during propagation. Extensive research [6–8] has been conducted on the interaction between Nesterenko solitary waves and local defect in a

granular chain. The most common approach to introduce such a defect is to replace one of the granules with a light intruder. It was shown that local intruders can significantly affect the nonlinear acoustics of granular media, through the generation of transient breathers that are localized at the sites of intruders and confine energy over relatively long-time scales.

The possibility of energy confinement in ordered granular media has led to investigations of granular protectors acting as energy absorbers. These consist of granular media that are designed to protect primary structures by absorbing energy from applied shock excitations, and only allowing drastically diminished excitations to reach the primary structures. A notable engineering application consists of layered granular materials separated by continuous elastic sheets used in retaining walls

E-mail address: chongan2@illinois.edu (C. Wang).

Corresponding author.

and reinforced by geogrid fabrics [9,10]. Such applications naturally lead to research on the nonlinear acoustics of granular-solid interfaces, since this can lead to predictive design and optimization of granular media as energy absorbers and shock mitigators. Potekin et al. [11] first developed an algorithm that accurately simulates the nonlinear wave scattering at the interface of a 1D granular chain with a linearly elastic cord, and Zhang et al. [12] extended this algorithm to the interface of a 1D granular chain with a linearly elastic membrane. In these algorithms, iterations and interpolations of the contact forces between at the granular-solid interfaces are applied at successive time steps to ensure their accurate computations. In both works, the 1D granular chains were composed of alternating heavy and light granules, i.e. they were granular dimmer. It was shown that the energy transmissibility at the discrete-continuum interface was highly dependent on the mass ratios of the alternating granules of the dimmers. Hence, by choosing the appropriate parameters, such 1D granular dimmer chains can be designed as effective passively shock mitigators.

Despite previous studies on 1D granular media, research on higherdimensional granular protectors is rather limited. In addition to typical Hertzian normal contact forces, tangential effects due to granular rotations are unavoidable in 2D or 3D granular media, which, in turn, lead to frictional effects that highly complicate the nonlinear acoustics. In fact, Yang et al. showed that the omission of frictional effects leads to significant errors [13] when modeling the acoustics of hexagonally packed granular media. Moreover, frictional effects may lead to dynamical instabilities [14-16], which represent an additional source of complication in the analysis in higher dimensions. Therefore, it is critical to accurately incorporate such frictional effects when studying 2D granular media as shock mitigators, as is the aim of the current work. Towards this aim, Wang et al. [17] extended the algorithm developed in [11] to 2D granular-elastic solid interfaces and achieved accurate simulations of the contact forces at the discrete-continuum interface, even when incorporating frictional effects due to granule rotations. The iterations of the contact forces at the interface between the granular medium and the elastic solid were conditionally stable when imposing a stability criterion which was formulated based on the forcing amplitudes, the adopted friction law and the variable time step increments. Therefore, sufficiently small time-steps were required for convergence of the computational iterations, thus ensuring the stability and robustness of the algorithm. This work paved the way for accurately and systematically studying the strongly nonlinear and highly discontinuous wave scattering at 2D granular-solid interfaces.

In the present work, we focus on the shock mitigation capacity of the granular medium component of a 2D granular-thin plate interface forced by shock excitation. The overall aim of the mitigation is to reduce as much as possible the portion of the shock energy that is eventually transmitted to the thin plate. Emphasis is given on the topological configuration and the geometric and material properties of the granular medium to efficiently localize the energy induced by applied shocks. Specifically, we consider a 2D granular medium composed of three layers of granules, being in contact with a thin plate (the elastic solid). Specifically, the granular medium is composed of two layers (columns) of "heavy" granules which are separated by an intermediate layer of "light" intruders. In Section 2, we briefly review the mathematical modeling of this granular-plate interface and explain the algorithm for the simulation. In Section 3, we evaluate the efficacy of the granular medium as shock mitigator and show that it can be designed to effectively localize (spatially confine) a major portion of the applied impulsive energy. Moreover, we show that shock mitigation in the granular medium can be maximized by appropriately selecting the system parameters of the layer of light intruders. Lastly in Section 4, we provide a brief synopsis of the main results of this work and discuss some possible future extensions.

2. System description

We consider 2D granular-solid interface shown in Fig. 1a, consisting of a granular medium in contact with a thin elastic plate. The granular medium is composed of 14 hexagonally packed granules arranged in two columns of heavy granules (granules 1-5 and A-E in Fig. 1b) and an intermediate column of light intruders (granules 6-9 in Fig. 1b), with no initial precompression. Each granule is spherical and composed of linear viscoelastic material. A distributed in-plane shock excitation is applied to the left column of the heavy granules, and the granularsolid interface is assumed to be at rest before the excitation is applied. For simplicity, only planar motions of the granules and the thin elastic plate - modeled using the plane stress approximation, are taken into consideration. The schematic of the 2D planar interface model is shown in Fig. 1b. All boundaries of the granular medium are assumed to be fixed (clamped) except for its right boundary granules that are in contact with the elastic plate. The top and bottom boundaries of the elastic plate are clamped as well, and the right boundary is tractionfree. In this work, we focus on the localization of a major portion of the applied shock energy to the granular medium. Accordingly, we study the primary wave transmission through the granular-solid interface, i.e., the transmission of the wave front that is generated immediately following the application of the shock. The overall aim is to reduce as much as possible the portion of the shock energy that is eventually transmitted to the thin plate. Following the methodology developed in previous works for similar discrete-continuum systems [11,12,17,18], the discrete element (DE) method is applied to model the granular medium, incorporating radial (Hertzian) and tangential (Frictional) interactions between granules, while the finite element (FE) method is employed to model the thin elastic plate. We note the Hertzian contact forces are generated due to granule-to-granule and granule-to-plate compressions, while frictional forces are due to granule rotations. These two computational models are coupled by accurately computing the interaction forces between the contacting boundary granules and the thin elastic plate at successive time steps through an iterative/interpolative computational algorithm. The validity of the computation is verified by the conservation of the total energy at each time step of the computation; this energy measure includes the energy dissipated by friction and the viscoelasticity of the granules.

The detailed DE and FE models for the components of the 2D granular interface granules have been described in detail in [14,15], so here we only provide a brief overview. Considering first the DE model of the granular medium, each granule is assumed to be linearly viscoelastic, but the strong nonlinearity in its acoustics is caused by (i) Hertzian interactions between granules when in compression [17, 18], (ii) separations between granules in the absence of compression and ensuing impacts between them, and (iii) frictional forces due to granule rotations; these nonlinearities also hold in the interactions of the boundary granules that are initially in contact with the elastic plate. Under certain conditions related to small deformations [19], each granule is modeled as a rigid body with three degrees of freedom (DOF), i.e. two translational and one rotational DOF. For sake of numerical stability [17], the frictional forces are modeled by the smooth Coulomb-tanh friction model [20,21]; as discussed in [14] using the non-smooth Coulomb friction law would lead to numerical instability of the simulations. Assuming that the ith granule is interacting with its neighboring jth granule and the elastic plate at the kth contact point (see Fig. 1c), its equations of motion are given by:

$$\ddot{s}_{i} = \frac{\sum_{j} \left(N_{ij} + f_{ij}\right) + \sum_{k} \left(N_{ik} + f_{ik}\right)}{m_{i}};$$

$$\ddot{\theta}_{i} = \frac{R_{i} \sum_{j} \left(n_{ij} \times f_{ij}\right) + R_{i} \sum_{k} \left(n_{ik} \times f_{ik}\right)}{I_{i}}$$
(1)

Referring to the notation of Fig. 1c, s_i denotes the displacement vector of the *i*th granule that involves the horizontal and vertical displacements; $\theta_i = \theta_i k$ is the rotational pseudo-vector of the *i*th granule where θ_i is the angle of rotation and k the unit pseudo-vector of the rotation

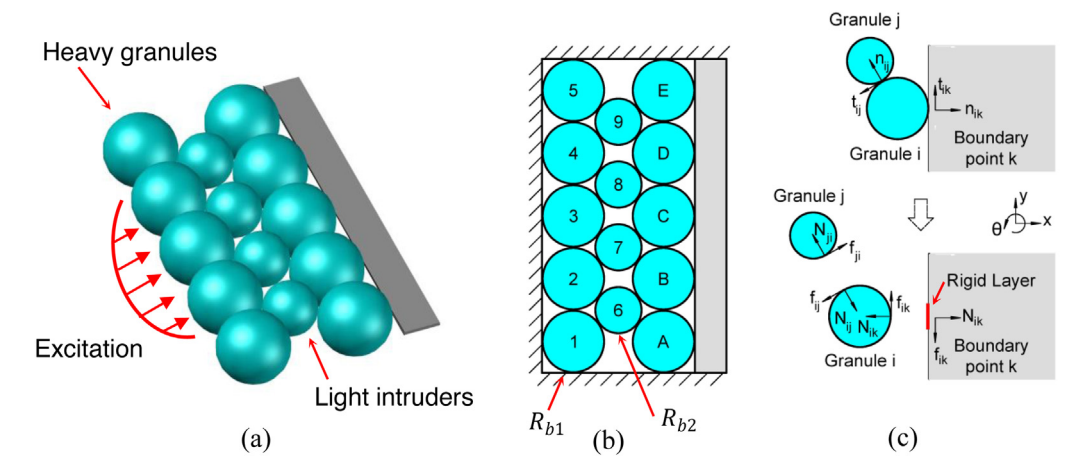


Fig. 1. Schematics of the granular-thin plate interface subject to a distributed shock excitation: (a) 3D isometric view, (b) 2D planar model with boundary conditions, and (c) granule-to-granule and granule-to-elastic plate contact points, corresponding free body diagrams and notations.

(with positive anti-clockwise direction); overdot denotes differentiation with respect to the time variable τ ; N_{ij} and f_{ij} are the normal and tangential forces, respectively, exerted to the ith granule by the jth granule; while N_{ik} and f_{ik} denote the normal and tangential forces exerted to the ith granule by the kth contact point at the interface with the plate. n_{ij} denotes the unit normal vector pointing from the center of the ith granule to the jth granule, while n_{ik} denotes the unit normal vector pointing from the center of the ith granule perpendicular to the kth boundary. In addition, m_i , R_i and $I_i = 2/5m_iR_i^2$ denote the mass, radius and moment of inertia of the ith granule, respectively.

The normal Hertzian forces in (1) are expressed as [13,22,23],

$$\mathbf{N}_{ij} = -\left(A_{ij}\delta_{n,ij}^{3/2} + \gamma_{ij}\dot{\delta}_{n,ij}\right)\mathbf{n}_{ij}
\mathbf{N}_{ik} = -\left(A_{ik}\delta_{nik}^{3/2} + \gamma_{ik}\dot{\delta}_{nik}\right)\mathbf{n}_{ik}$$
(2)

where $\delta_{n,ij} = max \left(R_i + R_j - \left| s_j - s_i \right|, 0 \right)$ is the relative normal deformation between the ith and the jth granules, and $\delta_{n,ik}$ is the relative normal deformation between the ith granule and the kth contact point with the plate; note that for the clamped boundaries, $\delta_{n,ik} = \left(s_i - s_i \left(\tau = 0 \right) \right) \cdot n_{ik}$. For simplicity, we only consider the translational motions of the flexible boundaries with the rotational motions neglected, which is valid in the limit of small deformations. Therefore, the normal vector n_{ik} is a constant for each flexible boundary, and $\delta_{n,ik} = \left(s_i - s_i \left(\tau = 0 \right) - u_k \right) \cdot n_{ik}$, where u_k denotes the displacement vector of the kth contact point on the plate. In (2) A_{ij} , γ_{ij} , (A_{ik} and γ_{ik}) denote the Hertzian and the viscous damping coefficients of the granule-to-granule contact (granule-contact point of the plate), respectively, given by:

$$A_{ij} = (4/3) E_{ij}^* \sqrt{R_{ij}^*}; \ A_{ik} = (4/3) E_{ik}^* \sqrt{R_{ik}^*}$$

$$\gamma_{ij} = \alpha_n \left(m_{ij}^* A_{ij} \right)^{1/2} \delta_{n,ij}^{1/4}; \ \gamma_{ik} = \alpha_n \left(m_{ik}^* A_{ik} \right)^{1/2} \delta_{n,ik}^{1/4}$$
(3)

In (3) α_n is a material coefficient related to the restitution coefficient [23], and E^* , m^* and R^* are the effective Young's modulus, mass and radius, respectively, given by:

$$\frac{1}{E_{ij}^*} = \frac{1 - v_i^2}{E_i} + \frac{1 - v_j^2}{E_j}, \qquad \frac{1}{E_{ik}^*} = \frac{1 - v_i^2}{E_i} + \frac{1 - v_k^2}{E_k},
\frac{1}{R_{ij}^*} = \frac{1}{R_i} + \frac{1}{R_j}; \frac{1}{R_{ik}^*} = \frac{1}{R_i} + \frac{1}{R_k}
\frac{1}{m_{ij}^*} = \frac{1}{m_i} + \frac{1}{m_j}, \qquad \frac{1}{m_{ik}^*} = \frac{1}{m_i} + \frac{1}{m_k}$$
(4)

In (4) E, v, R and m denote the Young's modulus, Poisson ratio, radius and mass of the granules or boundaries, and the subscripts i, j and k denote the ith granule, the jth granule and the kth contact point on the plate, respectively. For clamped boundaries, E_k , R_k , $m_k \to +\infty$ which

yields $E_{ik}^* = \frac{E_i}{1-v_i^2}$, $R_{ik}^* = R_i$ and $m_{ik}^* = m_i$ at the contact points between the granules and the three clamped boundaries. At the contact points between the granules and the elastic solid, we adopt the rigid layer model developed in [17,24] in order to overcome the inconsistency between the point contact and the plane-stress assumption of the elastic solid. Based on the rigid layer assumption, an artificial flat massless rigid layer is mounted on top of the elastic solid for each granular-solid contact point. In this case, $E_k \to +\infty$, $R_k \to +\infty$ and $m_k \to 0$ for the flexible boundaries, which yields $E_{ik}^* = \frac{E_i}{1-v_i^2}$, $R_{ik}^* = R_i$ and $m_{ik}^* = 0$ at the kth contact point on the boundary of the plate.

The Coulomb–tanh friction model [20,21] is used for the tangential forces applied to the granules (see Fig. 1c),

$$\mathbf{f}_{ij(ik)} = -\mu \left| \mathbf{N}_{ij(ik)} \right| \tanh \left(k_s \dot{\delta}_{t,ij(ik)} \right) \mathbf{t}_{ij(ik)} \tag{5}$$

where μ is the Coulomb friction coefficient, k_s a coefficient affecting the smoothness of the model, $t_{ij(ik)} = \mathbf{k} \times \mathbf{n}_{ij(ik)}$ the unit vector in the tangential direction, and $\dot{\delta}_{t,ij(ik)}$ the tangential relative velocity between the interacting granules or boundaries:

$$\dot{\delta}_{t,ij} = \left[\left(\dot{\mathbf{s}}_i + R_i \dot{\boldsymbol{\theta}}_i \times \mathbf{n}_{ij} \right) - \left(\dot{\mathbf{s}}_j + R_j \dot{\boldsymbol{\theta}}_j \times \mathbf{n}_{ji} \right) \right] \cdot \boldsymbol{t}_{ij}
\dot{\delta}_{t,ik} = \left[\left(\dot{\mathbf{s}}_i + R_i \dot{\boldsymbol{\theta}}_i \times \mathbf{n}_{ij} \right) - \dot{\boldsymbol{u}}_k \right] \cdot \boldsymbol{t}_{ik}$$
(6)

In (6) the velocity of the boundary point \dot{u}_k is equal to zero for the clamped boundaries and non-zero at the interface between the granular medium and the plate. A discussion on the assumptions and restrictions associated with the Coulomb–tanh friction model (5) is given in [14,15].

Considering now the FE model of the thin plate, the plane-stress approximation is invoked, which reduces the 3D linear elasticity equations to 2D by assuming $\sigma_z = \sigma_{xz} = \sigma_{yz} = 0$, where x and y denote the in-plane horizontal and vertical directions, and z denotes the direction along the thickness. Note that wave propagation in the (continuous) solid medium is much slower compared to wave propagation in the granular medium. Therefore, dissipation effects in the thin plate are neglected. The resulting governing 2D plane-stress equations were given in [14,15]. The FE method is then applied to discretize these equations by means of 8-node quadrilateral isoparametric elements. Special consideration is given to the rigid layers at the contact points between the boundary granules and the plate; to this end, the translational degrees of freedom of the middle points of the rigid layers are considered as the driving degrees of freedom, with the other nodes considered as the driven degrees of freedom following multi-point constraints [14]. At the end, the discretized equations of motion of the thin plate incorporating the rigid layers and the boundary conditions are expressed in the following form,

$$M\ddot{x} + Kx = F \tag{7}$$

where x denotes the displacement vector of the corresponding degrees of freedom, M and K global mass and stiffness matrices, respectively, and F contact force vector. We note that F is a sparse vector with non-zero elements equal to $-N_{ik}$ and $-f_{ik}$ located on the normal and tangential driving degrees of freedom of the rigid layer of the kth boundary on the plate. The components of the displacement vector corresponding to these degrees of freedom are equal to the normal and tangential components of the displacement vector of the kth boundary u_k .

The nonlinear DE equations (1) and the linear FE equations (7) are coupled through interaction force vector F between the boundary granules and the edge of the plate (see Fig. 1). Therefore, the accurate computation of these forces is crucial for the accurate simulations of the nonlinear acoustics. In the following computations the Newmark-beta method [25] is employed to simulate the FE equations (7), while the 4th order Runge-Kutta method is used to simulate the DE equation (1). Moreover, the interpolation-iteration algorithm developed in [11,17] is used to accurately compute the force vector F at successive time steps. For more details of the algorithm we refer to these works, but, in essence, the interaction force vector F is computed through the iteration of a high-dimensional global nonlinear map (as it contains the interaction forces at all contact points between the granular medium and the edge of the plate) whose stability is non-trivial. Following [17] this high-dimensional global nonlinear map is divided to a set of 1D local maps, each corresponding to the iteration of either the tangential or the normal interaction forces at each contact point; this reduction is valid as long as the effects of the interaction forces are local (i.e., the interaction forces at a contact point are decoupled from those at the other contact points), which is a valid assumption as long as the time step increment is sufficiently small. Therefore, the stability of the global map is reduced to the stability of the local maps. Since the frictional forces are sensitive to the relative tangential velocities, the stability of the map associated with the nonlinear iterations of the frictional forces is more critical compared to the normal (Hertzian) forces. Indeed, it is shown in [17] that the local map involving the iterations of the frictional force at a contact point is conditionally stable if the following

$$\left|\lambda_{ki,t}\right| = \frac{1}{2} \mu k_s \left| \boldsymbol{N}_{ik} \right| \Delta \tau \boldsymbol{T}_{i,t} \left(\boldsymbol{M} + \frac{1}{4} \boldsymbol{K} \Delta \tau^2 \right)^{-1} \boldsymbol{T}_{i,t}^{T} \cosh^{-2} \left(k_s \dot{\delta}_{t,ik} \right) < 1 \quad (8)$$

where $\lambda_{ki,t}$ denotes the eigenvalue of the linearized local map corresponding to the iteration of the tangential force between the ith granule and the kth boundary point on the plate (it turns out that numerical instabilities occur only at the frictional forces developing between the boundary granules in contact with the edge of the plate); $\Delta \tau$ denotes the time step increment at the given instant of the simulation, and $T_{i,t}$ a sparse vector with only one non-zero element equal to unity at the tangential driven DOF of the rigid layer at the kth boundary point on the plate [14]. The local map is stable if the modulus of the eigenvalue $|\lambda_{ki,t}|$ is smaller than unity, so at each time step of the simulation there exists a critical time step increment $\Delta \tau_{cr}$ that ensures stability provided that $\Delta \tau < \Delta \tau_{cr}$. In the following numerical simulations the self-adaptive algorithm developed in [17] is adopted by selecting the time step increment $\Delta \tau < \Delta \tau_{cr}$ thus ensuring the robust convergence of the computational algorithm at each time step. An example of the computational stability ensured by the criterion (8) for different contact points k is provided in Appendix A.

The accuracy of the simulation results is validated by checking the conservation of the total energy (including the dissipated energy) at each time step. The energy absorption (confinement) in the granular medium is studied by comparing the instantaneous energy transmitted to the plate, E_p , to the corresponding energy in the granular medium, E_v . These are computed as follows,

$$E_{p} = \frac{1}{2}\dot{\mathbf{x}}^{T}\mathbf{M}\dot{\mathbf{x}} + \frac{1}{2}\mathbf{x}^{T}\mathbf{K}\mathbf{x}$$

$$E_{g} = \sum_{i} E_{gi} = \sum_{i} \left(\frac{1}{2}m_{i} \left|\dot{\mathbf{s}}_{i}\right|^{2} + \frac{1}{2}I_{i}\dot{\theta}_{i}^{2} + \frac{1}{5}\sum_{j} A_{ij}\delta_{n,ij}^{5/2} + \frac{2}{5}\sum_{k} A_{ik}\delta_{n,ik}^{5/2}\right)$$

where E_{gi} denotes the instantaneous energy of the ith granule, composed of kinetic and potential energy components. Clearly, the total instantaneous energy E_p+E_g in the granular-solid interface monotonically decreases due to the dissipative effects. The total energy $D\left(\tau_0\right)$ dissipated up to the time instant τ_0 is evaluated by the work performed by the frictional (at the granule-to-granule and granule-to-plate interfaces) and viscoelastic forces (due to the material of the granules), $W_{\rm friction}\left(\tau_0\right)$ and $W_{\rm viscous}\left(\tau_0\right)$, respectively. These energy measures are computed as:

$$W_{\text{viscous}}(\tau_{0}) = \sum_{i}^{T} \int_{0}^{\tau_{0}} \left\{ \sum_{j} \left(\gamma_{ij} \dot{\delta}_{n,ij} \mathbf{n}_{ij} \cdot \dot{\mathbf{s}}_{i} \right) + \sum_{k} \left(\gamma_{ik} \dot{\delta}_{n,ik} \mathbf{n}_{ik} \cdot \dot{\mathbf{s}}_{i} \right) \right\} d\tau$$

$$W_{\text{friction}}(\tau_{0}) = \sum_{i}^{T_{0}} \left\{ \sum_{j} \left[\mathbf{f}_{ij} \cdot \left(\dot{\mathbf{s}}_{i} + R_{i} \dot{\theta}_{i} t_{ij} \right) \right] + \sum_{k} \left[\mathbf{f}_{ik} \cdot \left(\dot{\mathbf{s}}_{i} + R_{i} \dot{\theta}_{i} t_{ik} - \dot{\mathbf{u}}_{k} \right) \right] \right\} d\tau$$

$$(10)$$

$$D\left(\tau_{0}\right) = -W_{\text{viscous},i}\left(\tau_{0}\right) - W_{\text{friction},i}\left(\tau_{0}\right)$$

Hence, the total energy (including dissipated energy) at the time instant τ_0 , $E\left(\tau_0\right)$, should be conserved and equal to the energy induced by the shock, E_{shock} . It follows that the following relation should be checked at each time step of the simulation to ensure the accuracy of the computational results:

$$E_{p}\left(\tau_{0}\right) + E_{g}\left(\tau_{0}\right) + D\left(\tau_{0}\right) \equiv E\left(\tau_{0}\right) = E_{shock} \tag{11}$$

3. The granular interface as shock mitigator

In the following computational study, we focus on the capacity of the 2D granular interface as shock absorber and mitigator. As is shown in Fig. 1b, the left and right columns of the granular medium (composed of granules 1–5 and A–E, respectively) are composed of heavy granules with the radius R_{b1} , while the middle column consists of light intruders (granules 6–9) with radius $R_{b2} \leq R_{b1}$. Considering the hexagonal topology of the granular medium, since the light intruders should be in contact (fill the gap) with their neighboring heavy granules, it must also hold that $R_{b2} \geq \left(\sqrt{2}-1\right)R_{b1}$. In the following study the thin elastic plate and the heavy granules are composed of steel with Young's modulus E=200 GPa, Poisson ratio v=0.3 and density $\rho=7850$ kg/m³. The planar dimensions of the plate are 0.1 m×0.01 m, and its thickness is equal to 0.001 m. The radius of the heavy granules R_{b1} is equal to 0.01 m as well.

After the application of the shock, a primary wave is initiated in the granular medium, and as it transmits becomes dispersed and diminished in amplitude due to the highly discrete and strongly nonlinear nature of the granular interactions [14,15]. As a result, a drastically reduced and highly disintegrated set of primary weak waves reach the granular-plate interface, carrying a small portion of the initial shock energy. Therefore, we expect that the granular medium acts as a shock mitigator that significantly disintegrates the primary wave transmitted to the plate. The capacity of granular shock mitigation was investigated in 1D granular media that supports Nesterenko's solitary waves. One way to achieve the shock mitigation is to introduce a light intruder that scatters the solitary wave [7,24]. In the following study we aim to study the capacity for shock absorption 2D granular medium and establish its dependence on the geometric and material properties of the column of granular intruders. In this work, we consider the granularsolid hybrid system shown in Figs. 1b and 2b with three columns of granules, which is a highly degenerate case of 2D closely-packed granules. Even if the primary wave propagation in such 2D granular media deviates from Nesterenko's solitary waves in 1D homogeneous granular chains, the shock mitigation in such reduced 2D granular media is proven to be effective due to the primary wave disintegration. The design rules derived in this work can be extended to more complicated configurations.

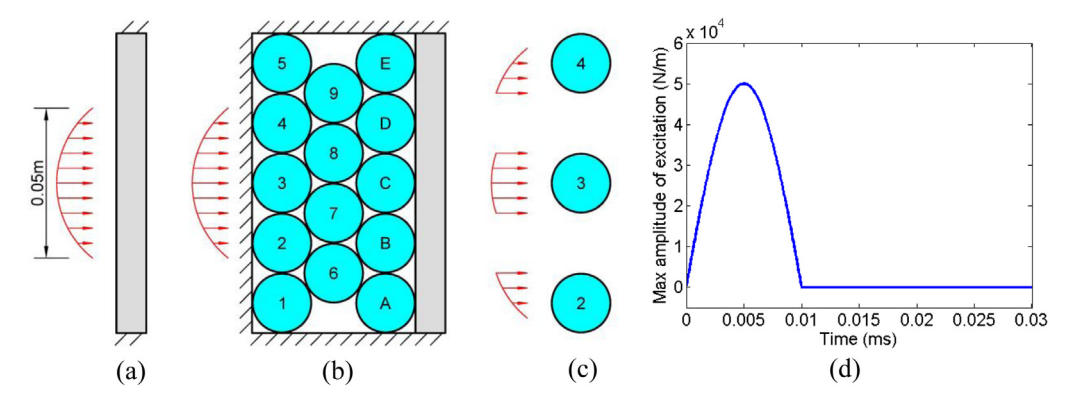


Fig. 2. Schematics of two different configurations: (a) Shock directly applied to the thin plate (no granular medium), (b) shock applied to the left column of the granular-solid interface, (c) force distributions on granules 2,3 and 4, and (d) temporal profile of the shock.

An indication of the shock mitigation capacity of the granular medium is gained by comparing the primary wave transmission through the granular interface to the case when an identical shock is directly applied to the plate (i.e., the granular medium is absent). In Fig. 2a, b we show the schematics of the two systems which are subject to the shock excitation depicted in Fig. 2c. The excitation consists of a half-sine pulse applied for a duration of 0.01 ms with a half-sine distribution in space, extending over 0.05 m in length. The peak of the shock excitation is equal to 50,000 N/m. In Fig. 2a, the excitation is directly applied to the free edge of the thin plate, whereas in Fig. 2b, it is applied to the left column of heavy granules; in the latter case, the forces are distributed only among granules 2, 3 and 4. The resultant excitation applied to granule 3 is equivalent to a horizontal concentrated force, while ones applied to granules 2 and 4 are equivalent to a combination of a horizontal force and torque since the centroids of the applied distributed forces do not coincide with the corresponding centroids of the granules. For this particular simulation, the intruders in the intermediate column of the granular medium are identical in size and material composition to their neighboring heavy granules, so we take $R_{h2} = 0.01$ m. Moreover, following the arguments of previous studies [13,17,23], the friction and viscoelastic damping coefficients are selected as $\mu = 0.099$, $\alpha_n = 6.313 \times 10^{-3}$ and $k_s = 1000$

The Von Mises yield criterion applies to ductile materials [26], stating that material yielding begins when the von Mises stress is greater than the yield stress. Therefore, in Fig. 3a, b we compare the maximum von Mises stresses in the thin plate versus time for the two cases subject to the shock excitation shown in Fig. 2c. The von Mises stress is given by,

$$\sigma_{VM} = \sqrt{\frac{1}{2} \left[\left(\sigma_{xx} - \sigma_{yy} \right)^2 + \left(\sigma_{yy} - \sigma_{zz} \right)^2 + \left(\sigma_{zz} - \sigma_{xx} \right)^2 \right] + 3 \left(\tau_{xy}^2 + \tau_{yz}^2 + \tau_{xz}^2 \right)}$$
(12)

where σ_{VM} denotes the von Mises stress; and σ_{xx} , σ_{yy} , σ_{zz} , τ_{xy} , τ_{yz} , au_{xz} denote the axial and shear components of the stress tensor. When the shock is directly applied to the plate the resulting maximum von Mises stress is ~350 MPa, which is close to the yield stress of steel. However, when the same shock is applied to the granular protector the resulting maximum von Mises stress drops significantly, reaching a maximum of just around ~80 MPa. This result provides a first hint on the capacity of the granular medium to significantly disperse the primary wave following the application of the shock, thus drastically reducing the remnant of the shock that eventually transmits through the plate. The drastic reduction of the von Mises stress is due to two main reasons: (i) The significant shock dispersion and disintegration at the granular medium and (ii) the reduction of the overall shock energy input in the granular interface compared to the case when the shock is applied directly to the plate. To demonstrate this, in Fig. 3c we depict the instantaneous energies of the granular system, the thin plate,

and the entire granular interface (with and without dissipative effects accounted for), normalized by the applied shock energy. The maximum energy in the plate is around 50% of the input shock energy, while the other 50% is scattered by the granular medium and not transferred to the elastic plate. However, the granular absorption does not fully account for the reduction of the von Mises stress. Apart from the energy scattering in the granular medium, the total shock energy input into the granular interface is significantly reduced compared to the case where the excitation is directly applied to the plate. Indeed, when the shock is directly applied to the plate, the total shock energy input is 1.53×10^{-2} J, while when the shock is applied to the granular interface, the input energy is 7.48×10^{-4} J, i.e., close to two orders of magnitude less. The large disparity in the input shock energy is achieved since the shock is applied to the heavy granules of the granular interface. Since the duration of the shock excitation is rather small, the energy exerted to a single granule can be approximated as $E_g = I_g^2/m_g$, where I_g is the magnitude of the applied impulse and m_{σ} the mass of the granule. In this case, the heavy granules are much heavier than the plate (i.e., the generalized mass of the first plate mode which is mainly excited [18]), so the input shock energy to the granular interface is much smaller.

In the next sections we will further explore the capacity of the granular medium for shock mitigation. Specifically, we will examine the effect of the intermediate column on the granular intruders on the shock dispersion and disintegration in the granular medium, in terms of the material composition (and the material disparity between the heavy granules and the intruders) and the size of the intruders. We will show that appropriate selection of the intruder column plays a crucial role in the shock mitigation capacity of the granular interface.

3.1. The effect of the intruder sizes on shock mitigation

We start by examining the effects of different intruder sizes on the shock transmission through the granular interface. Accordingly, we consider the intruder size $R_{b2} = 0.5R_{b1}$, i.e., we examine the case when the radii of the intruders are one-half of the radii of the heavy granules (see Fig. 1), and compare the results to the case when $R_{h2} = R_{h1}$ (when the intruder column is identical to its neighboring columns of heavy granules). The same half-sine distributed shock excitation shown in Fig. 2d is applied to the left column of heavy granules in both cases and investigate the corresponding responses of the granular interface. Moreover, in these simulations the friction and viscoelastic damping coefficients are still assigned the values $\mu = 0.099$, $\alpha_n = 6.313 \times 10^{-3}$ and $k_s = 1000$ s/m. We will be particularly interested in (i) the scattering by the granular medium of the primary shock wave front from the horizontal to the vertical direction, and (ii) the time scale disparity between the responses of the heavy granules and the light intruders due to the size disparity of the intruders.

The simulation results for $R_{b2} = 0.5R_{b1}$ are shown in Fig. 4b, d and f in comparison with the simulation results with $R_{b2} = R_{b1}$ shown in

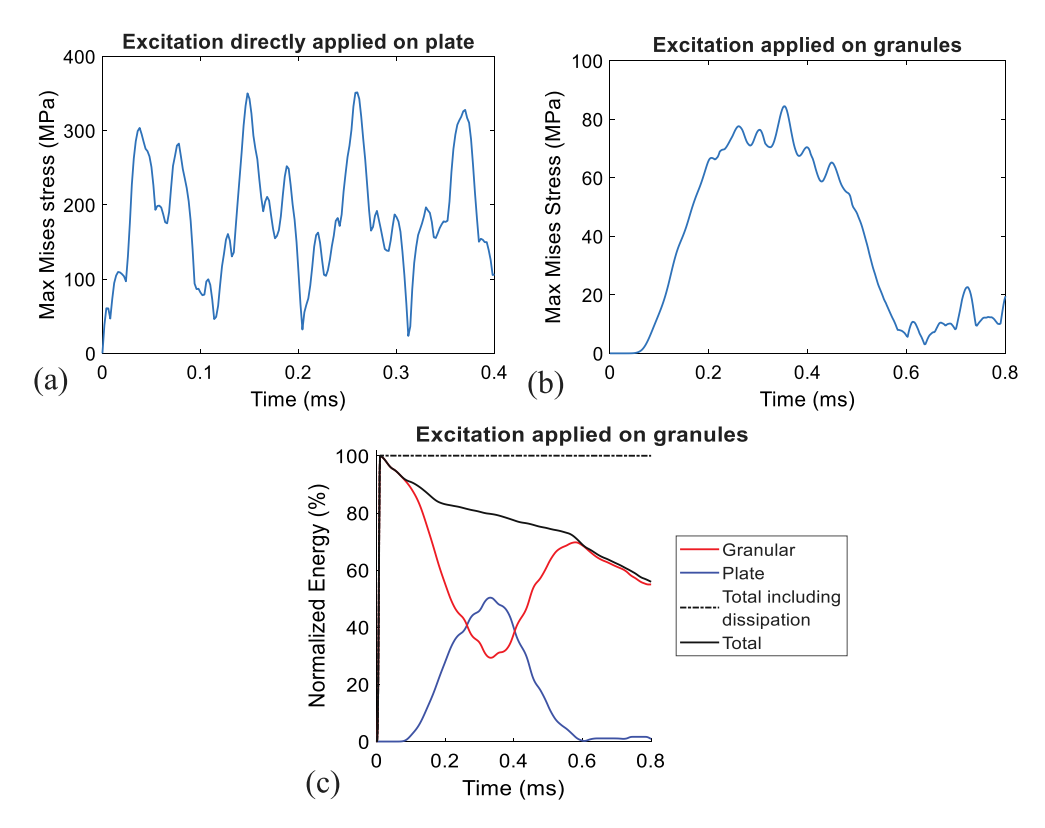


Fig. 3. Capacity of the granular medium for shock reduction: Maximum Mises stress in the plate (a) in the absence of the granular medium (see Fig. 2a), and (b) in the granular interface (see Fig. 2b); (c) instantaneous normalized energies of the granular interface (with and without dissipation taken into account) and of its constituent parts.

Fig. 4a, c and e. In Fig. 4a, b we compare the normalized instantaneous energies of the granular medium and the plate for the two intruder sizes. We deduce that the maximum normalized instantaneous energy transferred to the plate is over 50% for $R_{h2} = R_{h1}$, which is slightly reduced for $R_{h2} = 0.5R_{h1}$. In both cases, the initial impulsive energies of both cases are similar. In Fig. 4c, d we consider the total kinetic energy of the granular medium (including the intruders) for the two cases. The kinetic energy is partitioned into three parts, namely, the horizontal kinetic energy (in the axial direction of primary wave transmission), the vertical kinetic energy (in the direction orthogonal to the main wave transmission) and the rotational kinetic energy of the granules. Initially, only the horizontal and rotational kinetic energy components are excited in the granular medium. As the wave propagates, some energy is scattered from the horizontal to the vertical direction, so this part of the shock energy is diverted from reaching the plate. The energy scattering from the horizontal to the vertical directions is one of the mechanisms that disperse the shock energy within the granular medium. For smaller intruders, the angle of inclination between the centers of the heavy granules and the light intruders increases, and more energy is scattered from the horizontal to the vertical direction as is shown in Fig. 4d.

Apart from the aforementioned mechanism of energy scattering, we focus on the energy localization due to the disparity of the heavy granules and the light intruders, leading to an effective impedance mismatch. In Fig. 4e, f we compare the velocities of some representative heavy granules, namely granules 3 and C, together with the velocity of the representative light intruder 8. When $R_{b2} = R_{b1}$ the horizontal and vertical velocities of the intruder 8 oscillate with similar frequencies to the heavy granules 3 and C. This is not the case when $R_{b2} = 0.5R_{b1}$, where the intruders are lighter than the heavy granules; then the intruder oscillates at a faster time scale compared with the heavy granules, which indicates that the size difference leads to a fast/slow scale partition in the responses of the intruders and heavy granules, respectively. This leads to further improvement in the capacity of the

granular medium to localize a part of the shock energy, however, the overall improvement in shock mitigation is not high.

Hence, to further enhance the performance of the granular absorber we turn our focus into a lighter and softer material for the intruders thus increasing the disparity of mass and stiffnesses between the heavy granules and light intruders without varying the granule sizes. In the next section we show that this alternative intruder design yields to much more improved enhancement in the shock mitigation capacity of the granular interface.

3.2. The effect of the intruder material on shock mitigation

We proceed to study the capacity for shock mitigation of the granular interface when the column of intruders is composed of a different material compared to the neighboring columns of heavy granules. In order to increase the disparity of time scales between the responses of the heavy granules and the light intruders, we keep the size disparity by setting $R_{b2} = 0.5R_{b1}$, and, in addition, decrease the density and stiffness of the intruders by adopting a lighter and softer material. In this section, we consider polytetrafluoroethylene (PTFE) as the material of the light intruders in comparison to the steel heavy granules. The Young's modulus, Poisson ratio and density of PTFE are 0.54 GPa, 0.42 and 2.15×10^3 kg/m³, respectively. The friction coefficient at the steel-PTFE interface is set to $\mu = 0.099$. Since the material damping coefficient of PTFE is about one order of magnitude higher than the one of steel, we consider $\alpha_n = 6.313 \times 10^{-2}$ as the coefficient of viscoelastic damping for steel-PTFE contact interactions, which is nearly 10 times larger compared to the viscoelastic damping coefficient for steel-steel contact interactions.

In the following results the same half-sine distributed shock excitation shown in Fig. 2b is applied on the left column of the granules. The simulation results of the granular-solid interface with PTFE intruders in the leading 2 ms are shown in Fig. 5. The maximum deformations are checked for all PTFE intruders, and are much smaller (less than 1%)

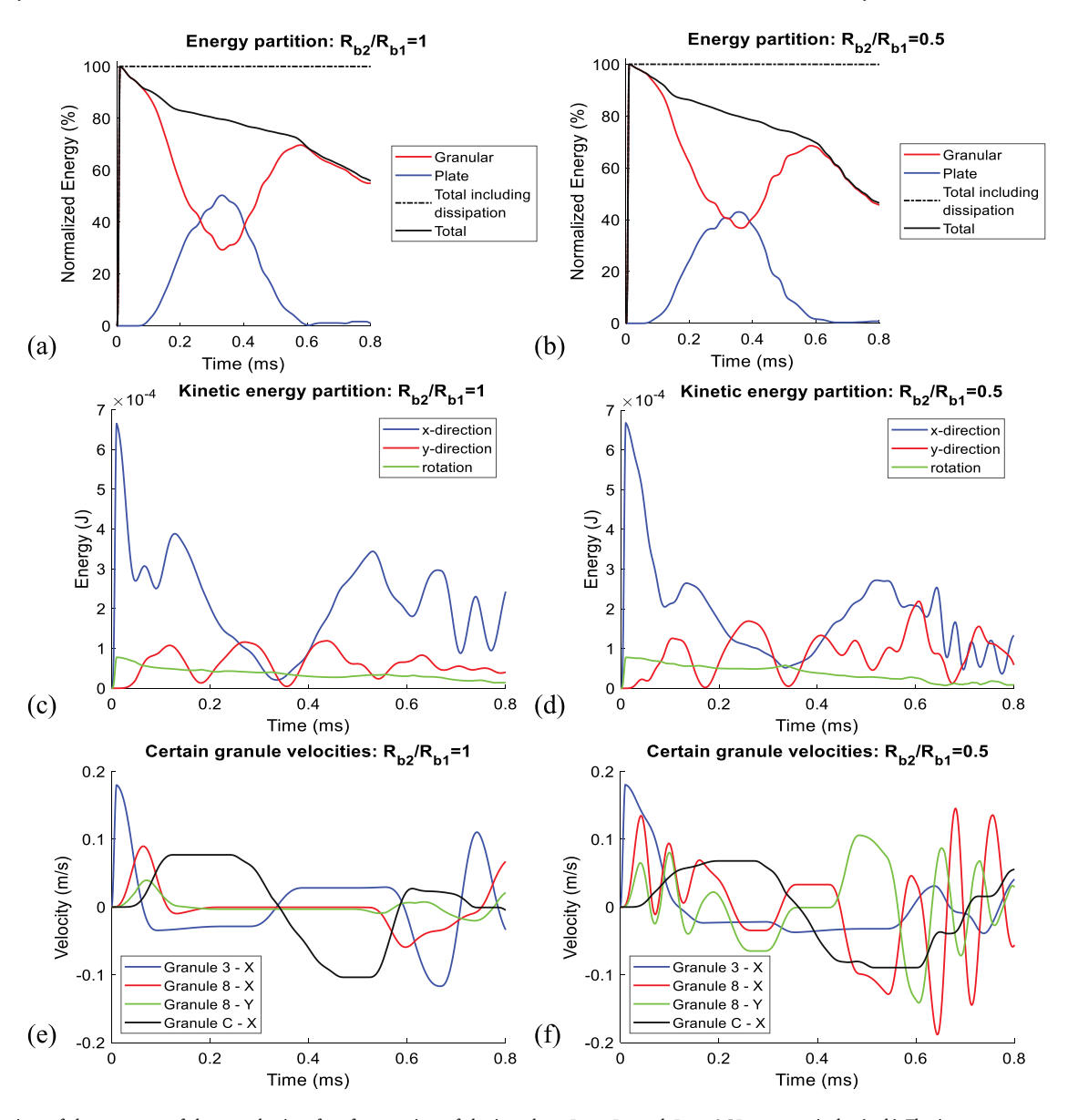


Fig. 4. Comparison of the responses of the granular interface for two sizes of the intruders, $R_{b2} = R_{b1}$ and $R_{b2} = 0.5R_{b1}$, respectively: (a, b) The instantaneous normalized energy partitions in the granular medium and the thin plate; (c, d) the instantaneous horizontal, vertical and rotational kinetic energy components in the granular medium; and (e, f) the horizontal and vertical velocities of granules 3, 8 and C (see Fig. 1b).

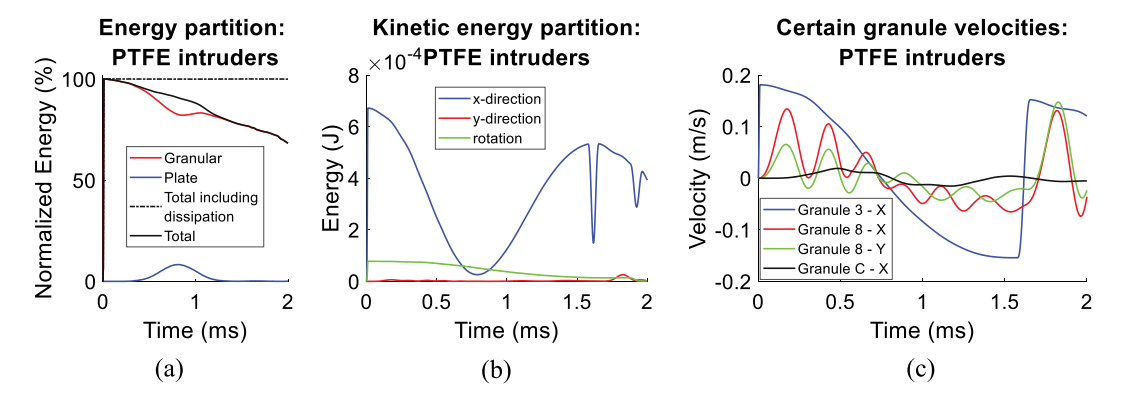


Fig. 5. Response of the granular interface for PTFE intruders: (a) The instantaneous normalized energy partition in the granular medium and the thin plate; (b) the instantaneous horizontal, vertical and rotational kinetic energy components in the granular medium; and (c) the horizontal and vertical velocities of granules 3, 8 and C (see Fig. 1b).

compared to the radius R_{b2} ; therefore the assumptions of the discrete granular model related to small deformations are still applicable in this

case. The normalized instantaneous energies of the granular medium, the plate and the overall granular interface are shown in Fig. 5a.

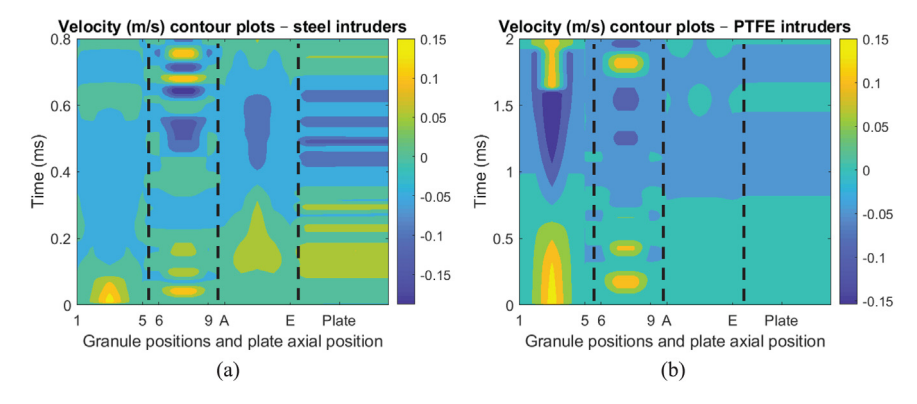


Fig. 6. Spatio-temporal evolutions of the horizontal (axial) velocity components (in m/s) of the granular interface: (a) Case of steel intruders, and (b) case of PTFE intruders.

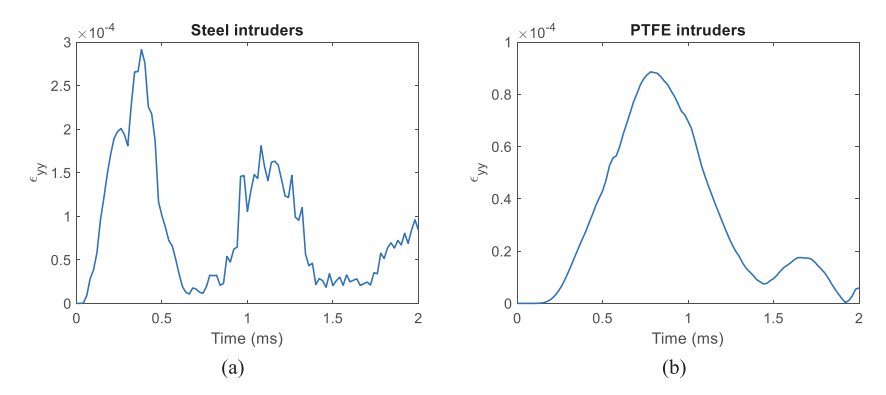


Fig. 7. Time evolutions of the maximum vertical strain components ε_{vv} in the thin plate, for (a) steel intruders, and (b) PTFE intruders.

Localization of shock energy in the granular medium is observed for PTFE intruders, which is in marked difference to the case of steel intruders (e.g., see Fig. 4a, b). Interestingly, in this case, only about 10% of the shock energy is eventually transmitted to the plate, therefore the granular medium provides much more effective shock mitigation compared to the case of same-size steel intruders, where as much as 40% of the shock energy is transmitted to the plate. We also note that the shock wave transmission is much slower with PTFE intruders, resulting from (i) the inhomogeneity of the granular medium and (ii) the low wave speed in PTFE due to its low Young's modulus.

Lastly, we note from Fig. 5c that the light intruder 8 oscillates with a similar amplitude compared to the heavy granule 3. However, the energy carried by the intruders is small due to their light weights, and so the energy transmitted through the intruder column is much smaller compared to the applied shock energy. In that same Fig. 5c we note that the oscillation amplitude of the heavy granule C, which is located on the third granular column, is much smaller compared with the amplitudes of the heavy granule 3 and the granular intruder 8; this further confirms the localization of shock energy mainly in the first granular column, and the incapacity for shock transmission through the granular medium in the case of PTFE intruders.

To intense shock energy localization (resulting in weak energy transmission to the plate) for the case of PTFE intruders is better highlighted in Fig. 6, where a comparison is also provided with the case of steel (same-size) intruders. The plots of Fig. 6 depict the spatiotempotal evolutions of the horizontal (axial) velocities of all granules and along the symmetric axis (in the axial direction) on the plate. In particular, the contour plots refer to the values of the axial velocities of the granules and points on the plate, and are divided into four parts; namely, (i) the first column of heavy granules labeled from 1 to 5, (ii) the column of light intruders labeled from 6 to 9, (iii) the third column of heavy granules labeled from A to E, and (iv) and the axial velocities on the symmetric axis of the thin plate (see Fig. 1b). Since the

top and the bottom boundaries of the plate are clamped, the maximum velocities occur at the middle of the plate, i.e., precisely on the selected symmetric axis of the plate.

In Fig. 6a (case of steel intruders) we notice that the horizontal velocities are varying in time in all the four columns, indicating that shock energy is transferred in the axial direction along the entire granular interface; clearly, in this case the localization of shock energy in the granular medium is small, although the intermediate column of steel intruders undergoes local oscillations, which, however, are not capable from restricting the axial transmission of the primary shock wave to the plate. As a result, a significant portion of shock energy is eventually transferred to the plate (see also Fig. 4b which corresponds to this case).

This is not the case for the softer PTFE intruders, where the shock energy is mainly localized in the first column of heavy granules, being incapable of transmitting along the axial direction (see Fig. 6b). This energy localization phenomenon is caused by the large effective impedance mismatch between the first column of heavy granules and the second column of light intruders, which results in an "effective barrier" for axial energy transmission along the granular interface; that is, the shock wave is effectively stopped at the interfaces between the heavy granules and the light intruders, so it becomes spatially confined in the first column of the heavy granule, close to the location of its generation. In this case the time scales of the granule oscillations and the wave transfer are different. With the steel intruders, the granules and the plate oscillate at faster frequencies compared to the case of PTFE intruders. Animations of all granular motions are provided in Appendix B, and these helps to better visualize the energy transfer and localization (or entrapment) for the cases of steel and PTFE intruders. At the same time, we note that the plate mainly undergoes bending vibrations, so in Fig. 7 we plot the maximum vertical strain component, ε_{vv} in the plate for both intruder cases. Clearly, by replacing the steel intruders with PTFE ones, the maximum vertical strain ε_{vv} is

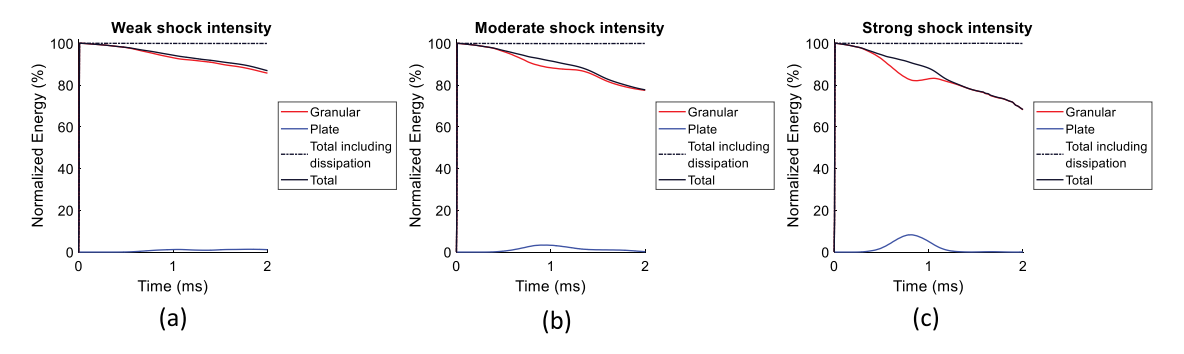


Fig. 8. Self-adaptivity of shock isolation on energy: Instantaneous normalized (with respect to the applied shock energy) energy partitions in the granular interface for (a) weak, (b) moderate, and (c) strong shock intensity.

significantly reduced, indicating the much better shock mitigation that is achieved for the plate for the case of PTFE intruders.

Lastly, we focus on an additional interesting feature of the nonlinear acoustics of the granular interface, namely, the dependence of the granular shock isolation capacity on the intensity of the applied shock excitation. This is to be expected due to the strong nonlinearity of the granular acoustics. To highlight this important feature, we vary the shock excitation considering different intensity loads. In the following simulations we consider exclusively the case of PTFE intruders with $R_{h2}/R_{h1} = 0.5$. Considering first a half-sine distributed shock excitation with a maximum amplitude of 50,000 N/m applied to the granular medium (see Fig. 2b), the maximum deformation of the PTFE intruders is close 1% of the radius R_{h2} so the discrete element model for the granular medium is valid even in this most severe loading case; this will be referred to as the "strong shock intensity" case. For comparison, we consider half-sine distributed excitations with the same spatial distributions but with smaller maximum amplitudes, namely, 10,000 N/m and 2000 N/m, which are referred to as the "moderate shock intensity" and the "weak shock intensity" cases, respectively. As shown in Fig. 8, the (passive) shock isolation capacity of the granular interface is self-adaptive to the shock excitation (or equivalently the energy level). Indeed, for the weak intensity case, the shock energy is almost completely localized in the granular medium (see Fig. 8a), however, as the intensity of excitation increases, an increasingly higher portion of the shock energy gets eventually transmitted to the thin plate (see Fig. 8b, c). Moreover, the governing time scales of the acoustics are also self-adaptive to the intensity of the shock, becoming faster for stronger excitations. Clearly, the self-adaptivity of the acoustics of the granular interface on the intensity of the shock excitations is due to the strong hardening nonlinearity of the Hertzian granule-to-granule and granuleto-plate interactions, so that the speed of the propagating wavefronts through the granular medium as well as the transmissibility of shock energy from the granular medium to the plate increase for stronger shock excitations.

4. Concluding remarks

We studied the shock mitigation capacity of 2D granular-thin plate interfaces subject to a half-sine shock excitation. Each interface consisted of an ordered granular medium — composed of two columns of heavy granules separated by an intermediate column of light intruders, interfacing with a thin plate. The shock excitation was applied to the left column of the granular medium and the overall aim of the mitigation was to reduce as much as possible the shock energy that was eventually transmitted to the thin plate. All hexagonally placed granules of the granular medium were initially uncompressed, giving rise to strongly nonlinear acoustics due to Hertzian contact interactions. With the plane-stress assumption for the thin plate, only planar stresses, forces and deformations were considered in these interfaces, so the acoustics was two-dimensional. The mathematical model developed for these complex, hybrid (discrete–continuum) systems incorporated

the highly nonlinear and discontinuous normal and tangential granule-to-granule and granule-to-plate interactions, individual granule rotations resulting in frictional effects, and the flexibility of the plate at its interface with the granular medium. The iterative/interpolative computational algorithm developed in [17] (based on the accurate computations of the contact forces at the discrete (granular) – continuum (plate) interfaces) was extended for the numerical simulations of the considered granular interfaces, with its stability being checked at each time instant through an appropriately formulated convergence criterion.

Comparing to the case where the shock excitation is applied directly on the plate (i.e., in the absence of the granular medium), it was demonstrated that the granular interface significantly reduced the maximum Mises stress in the thin plate. There are mainly two sources that account for this reduction: (i) Nearly 50% of the shock energy became locally confined in the granular medium and could not be transmitted to the plate, and (ii) the total input shock energy to the granular-plate interface was significantly reduced when it was applied to the granular medium.

Hence, we proceeded to design the granular medium (especially the intruder column) to maximize the proportion of shock energy that was eventually confined in it. To this end, intruders of different sizes and material compositions were considered. We hypothesized and systematically analyzed two possible ways to improve the shock mitigation capacity of the granular interface: (i) To "channel" the input shock energy from the axial direction (which was the main path of energy transfer) to a perpendicular direction within the granular medium, and (ii) to vary the impedance mismatch between the heavy granules and the light intruders.

For smaller sizes of the intruders, it was determined that more energy could be scattered from the axial to an orthogonal direction within the granular medium due to larger angles of inclination between the centers of the heavy granules and the intruders and their sizes were reduced. Moreover, the intruders oscillated with higher frequencies compared to the heavy granules, introducing a fast/slow mismatch in the corresponding responses. However, it was found that by just reducing the size of the intruders, the resulting energy localization of the shock energy in the granular medium was only improved slightly. As a second option, we considered different material compositions for the granular intruders, compared to the steel heavy granules. By replacing the light intruders with a softer and lighter polymeric material (PTFE), we found that much more energy could be localized in the first column of heavy granules. This was caused by the large impedance mismatch between the heavy granules and the light intruders, which prevented the energy transfer from the granular medium to the elastic plate; as a result, a major portion of the shock energy ended up being confined in the granular medium, with a very small portion being eventually transmitted to the thin plate. Hence, very effective shock mitigation was achieved in this case. Moreover, due to the strong nonlinearity of the governing acoustics, the shock mitigation capacity of the granular interface was shown to be self-adaptive to the intensity of the shock. In fact, weaker applied shocks lead to much more effective shock mitigation in the granular interface.

The considered shock energy mitigation due to impedance mismatch within the ordered granular medium could be considered as a 2D extension of previous 1D work in granular media. In that context, the present study acts as a first step towards predictively designing ordered granular interfaces for highly improved and self-adaptive to energy practical shock protectors. To this end, it would be of interest to extend the present study to granular interfaces composed of multiple granular layers, in three dimensions. This, for example, would be the case when one relaxes the thin plate assumption of the current work by considering plates (or other elastic media) with arbitrary thicknesses and more complex topologies.

CRediT authorship contribution statement

Chongan Wang: Writing codes, Perform numerical study of the research, Writing – original draft. **Sameh Tawfick:** Supervision, Revise the manuscript. **Alexander F. Vakakis:** Raise the question (idea), Supervision, Revise the manuscript.

Declaration of competing interest

The authors declare that they have no known competing financial interests or personal relationships that could have appeared to influence the work reported in this paper.

Acknowledgments

This work was supported in part by NSF Emerging Frontiers Research Initiative (EFRI) Grant 1741565. This support is gratefully acknowledged.

Appendix A. Example of the stability criterion (8)

Details of the computational algorithm can be found in [14,15] so they are not repeated. Here we demonstrate the stability of the algorithm through criterion (8) for the granular interface depicted in Fig. 2b, where the geometry and material properties of the intruders 6-9 are identical to the heavy granules in the first and third columns of the granular medium. It turns out that this is the most critical case (i.e., the most prone to numerical instability) considered in this work due to the strongest energy transfers between the granular medium and the plate. As in all simulations carried out in this work the initial time step increment is selected as $\Delta \tau_0 = 4 \times 10^{-8}$ s. In Fig. A.1, using an adaptive time step we plot the moduli of the eigenvalues (8) of the local maps for three of the five contact points between the boundary granules and the edge of the thin plate; this is sufficient due to the symmetry of the applied shock excitation, which, in turn, yields symmetry in the nonlinear acoustics of the granular interface. We note that the moduli of the eigenvalues are smaller than unity, ensuring the convergence of the computation at each time step.

Appendix B. Animations of the granular-elastic solid interface for PTFE or steel intruders

Here we provide links to animations of the responses of the granular-solid interface for the cases of PTFE or steel intruders. The radii of the intruders are equal to half of the radii of the heavy granules, and a half-sine shock with a peak of 50 000 N/m is applied to the left column of the granular medium. In the animations the displacements of the granule and the boundaries of the thin plate are magnified by 125 times. For steel intruders the shock transmits rapidly through the granular medium, reaching the edge of the plate (and transmitting through it) in a relatively short time; in this case, the

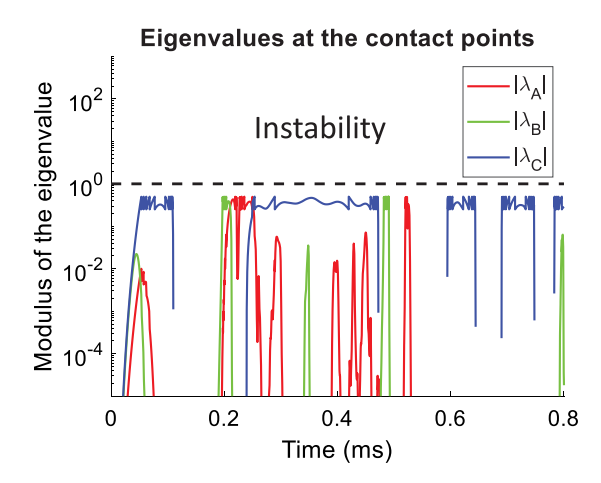


Fig. A.1. Variations of the moduli of the eigenvalues (8) for the local maps of the frictional forces at the contact points between the boundary granules A, B and C and the edge of the plate — see Fig. 2b.

first column of heavy granules transmits shock energy to the second column through the intermediate column of granular intruders, which, in turn, transmits a portion of the shock energy eventually to the plate (see Fig. 6a). The nonlinear acoustics is drastically different for PTFE intruders, where the shock energy is mainly localized in the first granular column of heavy granules and only a small amount of the shock energy eventually reaches the second column of heavy granules and the plate (see Fig. 6b).

Animation of the granular-solid interface with steel intruders (magnified \times 125):

https://uofi.box.com/s/9g1042spvbvu351bc7w70yvuy7l49gkm

Animation of the granular-solid interface with PTFE intruders (magnified \times 125):

https://uofi.box.com/s/ami30mq99rflnf9rgpyfruxns37biz5d

References

- A. Lazaridi, V. Nesterenko, Observation of a new type of solitary waves in a one-dimensional granular medium, J. Appl. Mech. Tech. Phys. 26 (3) (1985) 405–408
- [2] V. Nesterenko, Dynamics of Heterogeneous Materials, Springer Verlag, New York, 2001.
- [3] V. Nesterenko, Propagation of nonlinear compression pulses in granular media, J. Appl. Mech. Tech. Phys. 24 (5) (1983) 733–743.
- [4] V. Nesterenko, Solitary waves in discrete media with anomalous compressibility and similar to sonic vacuum, in: EURODYMAT 1994-4th International Conference on Mechanical and Physical Behaviour of Materials under Dynamic Loading, Oxford, 1994.
- [5] S. Sen, J. Hong, J. Bang, E. Avalos, R. Doney, Solitary waves in the granular chain, Phys. Rep. 462 (2) (2008) 21–66.
- [6] E. Hascoët, H.J. Herrmann, Shocks in non-loaded bead chains with impurities, Eur. Phys. J. B 14 (1) (2000) 183–190.
- [7] S. Job, F. Santibanez, F. Tapia, F. Melo, Wave localization in strongly nonlinear Hertzian chains with mass defect, Phys. Rev. E 80 (2) (2009) 025602.
- [8] G. Theocharis, M. Kavousanakis, P.G. Kevrekidis, C. Daraio, M.A. Porter, I.G. Kevrekidis, Localized breathing modes in granular crystals with defects, Phys. Rev. E 80 (6) (2009) 066601.
- [9] G. Yang, B. Zhang, P. Lv, Q. Zhou, Behaviour of geogrid reinforced soil retaining wall with concrete-rigid facing, Geotext. Geomembr. 27 (5) (2009) 350–356.
- [10] L. Wang, G. Chen, S. Chen, Experimental study on seismic response of geogrid reinforced rigid retaining walls with saturated backfill sand., Geotext. Geomembr. 43 (1) (2015) 35–45.
- [11] R. Potekin, D. McFarl, A. Vakakis, Nonlinear wave scattering at the flexible interface of a granular dimer chain, Granul. Matter 18 (3) (2016) 1–17.
- [12] Q. Zhang, R. Potekin, W. Li, A. Vakakis, Nonlinear wave scattering at the interface of granular dimer chains and an elastically supported membrane, Int. J. Solids Struct. 182 (2020) 46–63.
- [13] J. Yang, M. Sutton, Nonlinear wave propagation in a hexagonally packed granular channel under rotational dynamics, Int. J. Solids Struct. 77 (2015) 65–73.

- [14] C. Goldenberg, I. Goldhirsch, Friction enhances elasticity in granular solids, Nature 435 (7039) (2005) 188–191.
- [15] J. Chattoraj, O. Gendelman, M. Ciamarra, I. Procaccia, Oscillatory instabilities in frictional granular matter, Phys. Rev. Lett. 9 (098003) (2019) 123.
- [16] H. Charan, O. Gendelman, I. Procaccia, Y. Sheffer, Giant amplification of small perturbations in frictional amorphous solids, Phys. Rev. E 101 (6) (2020) 062902.
- [17] C. Wang, Q. Zhang, A. Vakakis, Wave transmission in 2D nonlinear granularsolid interfaces, including rotational and frictional effects, Granul. Matter 23 (2) (2021) 1–24.
- [18] C. Wang, S. Tawfick, A.F. Vakakis, Time scale disparity yielding acoustic nonreciprocity in a two-dimensional granular-elastic solid interface with asymmetry, Phys. Rev. E 104 (4) (2021) 044906.
- [19] Y. Starosvetsky, K. Jayaprakash, M. Hasan, A. Vakakis, Topics on the Nonlinear Dynamics and Acoustics of Ordered Granular Media, World Scientific Press, Singapore, 2017.

- [20] S. Andersson, A. Söderberg, S. Björklund, Friction models for sliding dry, boundary and mixed lubricated contacts, Tribol. Int. 40 (4) (2007) 580–587.
- [21] E. Pennestrì, V. Rossi, P. Salvini, P. Valentini, Review and comparison of dry friction force models, Nonlinear Dynam. 83 (4) (2016) 1785–1801.
- [22] P. Cundall, O. Strack, A discrete numerical model for granular assemblies, Geotechnique 29 (1) (1979) 47–65.
- [23] Y. Tsuji, T. Tanaka, T. Ishida, Lagrangian numerical simulation of plug flow of cohesionless particles in a horizontal pipe, Powder Technol. 71 (3) (1992) 239–250.
- [24] Y. Starosvetsky, A. Vakakis, Primary wave transmission in systems of elastic rods with granular interfaces, Wave Motion 48 (7) (2011) 568–585.
- [25] S. Timoshenko, J. Goyder, Theory of Elasticity, third ed., McGraw Hill, New York, 2010.
- [26] N.M. Newmark, A method of computation for structural dynamics, J. Eng. Mech. Div. 85 (3) (1959) 67–94.